J. Fluid Mech. (1966), *vol.* 26, *part* 1, *pp.* 163–182
Printed in Great Britain

The integration of the two-dimensional laminar boundary-layer equations past the point of vanishing skin friction

By D. CATHERALL AND K. W. MANGLER
Aerodynamics Department, Royal Aircraft Establishment, Farnborough, Hants.

(Received 27 September 1965 and in revised form 25 January 1966)

A method is proposed for obtaining regular solutions of the boundary-layer equations near a point of vanishing skin friction for steady incompressible laminar two-dimensional flow. The boundary-layer equations are integrated numerically in the usual way until the separation point is approached; then the displacement thickness is prescribed as a regular function of the distance along the surface, leaving the pressure gradient to be calculated from the consequent solution. Numerical solutions are obtained with reversed flow and shallow separation bubbles inside the boundary layer without the occurrence of a singularity at the separation point.

1. Introduction

It is well-known that the flow field past a solid body can be divided into a boundary layer and an inviscid irrotational flow outside it. The latter is determined not by the solid surface itself but by a surface displaced into the fluid through a distance δ_1, the 'displacement thickness' of the boundary layer. For very large Reynolds numbers R the boundary-layer thickness before separation is of order λ ($\lambda = R^{-\frac{1}{2}}$) and so δ_1 is of order λ and in the limit of infinite Reynolds number the displacement surface up to separation is coincident with the body so that (as is the usual procedure) the pressure distribution may be taken from the potential flow about the body and then the boundary layer can be calculated using 'stretched' variables. In this solution the 'stretched' displacement thickness $\bar{\delta}_1$ ($\bar{\delta}_1 = \delta_1/\lambda$) is of order unity.

Whenever the pressure gradient along the surface becomes adverse (positive gradient) the skin friction decreases until eventually it becomes zero and the forward flow separates from the wall. Beyond the point of separation the flow direction is reversed near the wall and either a small bubble is formed inside the boundary layer or the boundary layer thickens considerably producing a large bubble or a thick wake. The flow downstream of separation may influence the pressure distribution upstream and thus the position of the separation point. However, so far no satisfactory model of the flow downstream of separation under these conditions has been found and so this influence is extremely difficult to assess. In many practical cases this upstream influence of separation on the pressure distribution is small and for the forward part of the body the pressure

distribution obtained from the potential flow past the given body is adequate. Near separation this is no longer true and an alternative method will be proposed.

After separation the boundary-layer thickness may remain of order λ, leading to the formation of a shallow bubble inside the boundary layer or (as is often observed experimentally) it may become of order unity. In the former case the upstream effect on the pressure distribution is very small, whereas in the latter case it becomes important; furthermore, $\bar{\delta}_1$ will change from being of order unity before separation to of order λ^{-1} after separation, which, in the limit as λ tends to zero, means that $\bar{\delta}_1$ will become infinite after separation. The boundary-layer equations will, of course, no longer be valid after separation in this case, since the approximations made in forming the boundary-layer equations assume that $\bar{\delta}_1$ is of order unity, and it may be expected that a singularity will be present in the boundary-layer equations at the separation point.

All numerical computations in which any attempt has been made to obtain good accuracy, at and near separation, have so far met with considerable difficulty, and this also has led to the conclusion that the boundary-layer equations for laminar incompressible flow do indeed have a singularity at the separation point. The nature of this singularity has been studied by Goldstein (1948), Stewartson (1958), Terrill (1960) and Catherall, Stewartson & Williams (1965), and solutions valid in the neighbourhood of the separation point have been obtained which give a singularity in the skin friction at the point of separation.

In this paper we try to make allowance for the effect on the pressure distribution of a small bubble inside the boundary layer. We assume that the displacement thickness behaves in a regular prescribed fashion in the region of the separation point and the pressure distribution is calculated in this region at the same time as the boundary-layer calculation is performed. This leads to a numerical solution which does not show any signs of a singular behaviour at separation.

In § 2 the Navier–Stokes equations for two-dimensional incompressible flow are written in terms of a stream function and the vorticity, and in § 3 a transformation is introduced in which the independent variables are simply connected to the inviscid stream function and velocity potential. This system is most convenient when considering higher approximations in boundary-layer theory, but for this paper, since only the limit of infinite Reynolds number is considered, the system is equivalent to Prandtl's boundary-layer equations. The equivalence is demonstrated in § 3. Stagnation-point flow is considered in § 4 and the numerical integration of the equations† is briefly described in § 5. Various examples are given in § 6, the first one being merely an illustrative one of the flow past a parabola to check the numerical method, and then the technique described in the last paragraph is employed to integrate past separation. An example is also given of a shallow bubble contained inside the boundary layer, no difficulty being encountered at either separation or reattachment. It should be noted, though, that the solution after separation is not uniquely determined unless boundary conditions are supplied downstream, the physical reason being that disturbances can

† A more complete description of the numerical method, including a series solution for the stagnation-point region, is contained in an unpublished R.A.E. report.

propagate upstream once reversed flow has set in. However, for the latter case of a shallow bubble it was concluded that all possible solutions lay within a range narrower than the accuracy of the calculation.

The technique will only work, of course, for regions where the boundary-layer thickness remains of order λ. Shallow bubbles within the boundary layer do occur; for example, they are often present when a shock wave interacts with the boundary layer, and the possibility also remains that the strong thickening of the boundary layer after separation may sometimes occur some finite distance downstream of the separation point. If this were the case the present method would still enable one to integrate the boundary-layer equations past the separation point.

2. Equations of motion and boundary conditions

In Cartesian co-ordinates (x, y) the two-dimensional steady incompressible Navier–Stokes equations are (in non-dimensional form)

$$u\frac{\partial u}{\partial x}+v\frac{\partial u}{\partial y}=-\frac{\partial p}{\partial x}+\lambda^2\left(\frac{\partial^2 u}{\partial x^2}+\frac{\partial^2 u}{\partial y^2}\right), \tag{1}$$

$$u\frac{\partial v}{\partial x}+v\frac{\partial v}{\partial y}=-\frac{\partial p}{\partial y}+\lambda^2\left(\frac{\partial^2 v}{\partial x^2}+\frac{\partial^2 v}{\partial y^2}\right), \tag{2}$$

$$\frac{\partial u}{\partial x}+\frac{\partial v}{\partial y}=0, \tag{3}$$

where the x and y components of velocity u and v have been non-dimensionalized with respect to the undisturbed velocity U_∞, the pressure p with respect to ρU_∞^2 (ρ = density) and all lengths with respect to a typical body dimension (such as the nose radius) L. λ is connected to the Reynolds number R through

$$R=\rho U_\infty L/\mu \equiv \lambda^{-2}, \tag{4}$$

where μ is the coefficient of viscosity.

Equation (3) is satisfied by introducing a stream function ψ, where

$$u=\partial\psi/\partial y, \quad v=-\partial\psi/\partial x. \tag{5}$$

Eliminating p between (1) and (2) and introducing the vorticity ω, where

$$-\omega=(\partial u/\partial y)-(\partial v/\partial x), \tag{6}$$

the Navier–Stokes equations may be reduced to two equations:

$$\frac{\partial\psi}{\partial y}\frac{\partial\omega}{\partial x}-\frac{\partial\psi}{\partial x}\frac{\partial\omega}{\partial y}=\lambda^2\left(\frac{\partial^2}{\partial x^2}+\frac{\partial^2}{\partial y^2}\right)\omega, \tag{7}$$

$$-\omega=\left(\frac{\partial^2}{\partial x^2}+\frac{\partial^2}{\partial y^2}\right)\psi. \tag{8}$$

The boundary conditions are the 'no-slip' conditions

$$u=v=0 \tag{9}$$

along the body $y=y_B(x)$, and

$$u=1, \quad v=0 \tag{10}$$

at large distances from the body and outside the wake, the undisturbed stream being assumed to be flowing in the x-direction.

For large Reynolds number, large parts of the flow field are not affected by viscosity and can be described by the Euler equations for inviscid flow. The velocity components U, V of the inviscid flow past the displacement surface S_D (figure 1) can be defined in terms of a stream function χ and velocity potential ϕ:

$$U = \frac{\partial \chi}{\partial y} = \frac{\partial \phi}{\partial x}, \quad V = -\frac{\partial \chi}{\partial x} = \frac{\partial \phi}{\partial y}. \tag{11}$$

When we come to take the limit of infinite Reynolds number, this distinction between defining the inviscid flow to be about the displacement surface rather than the body surface S_B disappears.

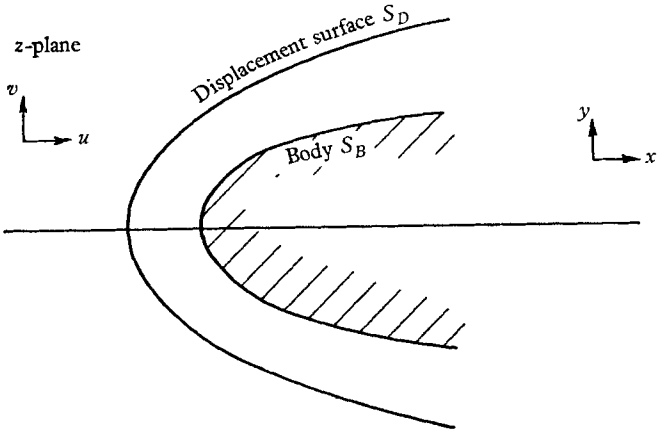

FIGURE 1. Physical plane showing body surface S_B and displacement surface S_D before limit $\lambda \to 0$ taken.

3. Change of variables

Orthogonal co-ordinates X and Y are introduced connected to ϕ and χ by

$$\phi + i\chi = \tfrac{1}{2}Z^2, \tag{12}$$

where $Z = X + iY$, so that

$$\phi = \tfrac{1}{2}[X^2 - Y^2], \quad \chi = XY. \tag{13}$$

The implied transformation from (x, y) space to (X, Y) space is

$$z = z(Z), \tag{14}$$

say, where $z = x + iy$, and the inviscid complex velocity, $U - iV = q e^{-i\tau}$, where q is the magnitude, and τ represents the direction, of the velocity vector, is given by

$$q e^{-i\tau} = \frac{d}{dz}(\phi + i\chi) = Z \Big/ \frac{dz}{dZ}. \tag{15}$$

The Jacobian J of the transformation, which is the ratio between elements of area in the z- and Z-planes is

$$J = |dz/dZ|^2 = (X^2 + Y^2)/q^2. \tag{16}$$

In the Z-plane the streamlines of the inviscid flow are (from the second equation in (13))

$$XY = \text{const.}; \tag{17}$$

the displacement surface is $Y = 0$, and the body is $Y = Y_B(X) < 0$ (figure 2). X and Y are measured along and perpendicular to the displacement surface in the Z-plane.

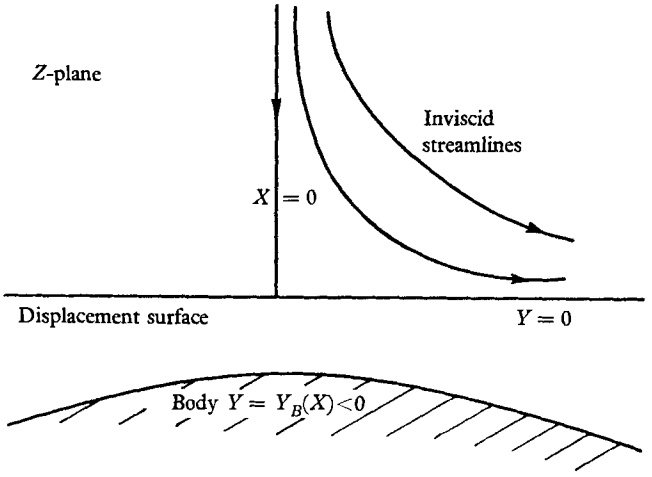

FIGURE 2. Inviscid flow picture mapped onto Z-plane before limit $\lambda \to 0$ taken.

Under this transformation we find

$$\left.\begin{aligned} dx &= \frac{XU - YV}{q^2}\,dX - \frac{(XV + YU)}{q^2}\,dY, \\ dy &= \frac{XV + YU}{q^2}\,dX + \frac{(XU - YV)}{q^2}\,dY. \end{aligned}\right\} \tag{18}$$

It may be noted here that since $U - iV$ is an analytic function of Z for $Y \geqslant 0$, U and V are not independent. In fact it is only necessary to prescribe U, say, along $Y = 0$ for both U and V to be defined throughout the whole of the region $Y \geqslant 0$, from Cauchy's integral theorem.

In this system the Navier–Stokes equations (7) and (8) become

$$\frac{\partial \psi}{\partial Y}\frac{\partial \omega}{\partial X} - \frac{\partial \psi}{\partial X}\frac{\partial \omega}{\partial Y} = \lambda^2 \left(\frac{\partial^2}{\partial X^2} + \frac{\partial^2}{\partial Y^2}\right)\omega, \tag{19}$$

$$-J\omega = \left(\frac{\partial^2}{\partial X^2} + \frac{\partial^2}{\partial Y^2}\right)\psi. \tag{20}$$

The variable Y is now 'stretched' in an analogous way to Prandtl's 'stretching' of the direction perpendicular to the wall. We write

$$X = \xi, \quad Y = \lambda\eta; \tag{21}$$

and

$$\psi = \lambda\xi(\eta + H), \quad \omega = \xi\bar{\omega}/\lambda. \tag{22}$$

Note here that we assume that the stagnation streamline coincides with the line $\xi = 0$, the inviscid stagnation streamline. This will only be true for symmetrical

flows (for non-symmetrical flows the inviscid stagnation streamline is deformed by the displacement effect due to the viscous layer and the stagnation point may be shifted).

The first term in the expression for ψ in (22) represents the inviscid solution $\psi = \chi$ and the second term $\lambda\xi H = \lambda\psi^*$ the viscous modification to the inviscid flow, so that if we make H decay as we move from the body into the main stream the solution will merge into the external potential flow solution.

Writing equations (19) and (20) in terms of these new variables and letting $\lambda \to 0$ (i.e. $R \to \infty$) we have

$$\left(1+\frac{\partial H}{\partial \eta}\right)\frac{\partial(\xi\overline{\omega})}{\partial \xi} - \left(\eta + \frac{\partial(\xi H)}{\partial \xi}\right)\frac{\partial \overline{\omega}}{\partial \eta} = \frac{\partial^2 \overline{\omega}}{\partial \eta^2}, \tag{23}$$

$$-J\overline{\omega} = \frac{\partial^2 H}{\partial \eta^2}. \tag{24}$$

The body itself is given by $\eta = \eta_B(\xi)$ and the 'no slip' conditions are $\psi = \partial\psi/\partial\eta = 0$ on the body. Thus the boundary conditions for equations (23), (24) are

$$H = -\eta_B, \quad \partial H/\partial \eta = -1 \quad \text{on} \quad \eta = \eta_B, \tag{25}$$

and both H and $\overline{\omega}$ decay exponentially for large η.

These may be considered as the equations for the first term in an expansion of H in powers of λ, following Van Dyke (1962, 1964), or alternatively they may be considered as the equations for infinite Reynolds number flow.

Before attempting to solve (23) and (24) we need to know the function J which depends on the velocity $q = q(\xi, \lambda\eta)$ of the flow past S_D. We may expand q in a Taylor series in the η-direction, and since it is known that for smooth bodies $(\partial q/\partial(\lambda\eta))_{\eta=0} = (\partial q/\partial Y)_{\eta=0}$ is of order 1 we may write

$$q = q(\xi, 0) + O(\lambda), \tag{26}$$

and from (16), (21) and (26) we have

$$J = \frac{\xi^2}{(q(\xi,0))^2} + O(\lambda). \tag{27}$$

As mentioned in the introduction, this co-ordinate system, since it is based on the inviscid flow about the displacement surface, is most convenient when considering higher-order effects in boundary-layer theory, where the function H is expanded in a power series in λ and the inviscid and viscous parts of the flow are made to merge into each other simply by making H decay exponentially with distance from the surface. However, for the limiting case of infinite Reynolds number which has been taken equations (23) and (24) are the equivalent of Prandtl's boundary-layer equations, which can be obtained from (23) and (24) by use of the following transformation:

$$\left.\begin{aligned} \tilde{x} = \int_0^{\xi} J^{\frac{1}{2}}\, d\xi, \quad \tilde{y} = J^{\frac{1}{2}}(\eta - \eta_B), \\ \tilde{\psi} = \xi(\eta + H), \end{aligned}\right\} \tag{28}$$

where J is given by (27). The governing equations reduce to

$$\frac{\partial\tilde{\psi}}{\partial\tilde{y}}\frac{\partial^2\tilde{\psi}}{\partial\tilde{x}\,\partial\tilde{y}}-\frac{\partial\tilde{\psi}}{\partial\tilde{x}}\frac{\partial^2\tilde{\psi}}{\partial\tilde{y}^2}=q\frac{dq}{d\tilde{x}}+\frac{\partial^3\tilde{\psi}}{\partial\tilde{y}^3} \tag{29}$$

with boundary conditions

$$\left.\begin{aligned}\tilde{\psi}=\frac{\partial\tilde{\psi}}{\partial\tilde{y}}=0 \quad &\text{at} \quad \tilde{y}=0,\\ \frac{\partial\tilde{\psi}}{\partial\tilde{y}}\to q \quad &\text{as} \quad \tilde{y}\to\infty.\end{aligned}\right\} \tag{30}$$

In this formulation the unknown function η_B, which is connected to the displacement thickness ($-\eta_B=\delta_1/\lambda J^{\frac{1}{2}}$) does not occur explicitly and it is doubtful whether integration past the separation point by specifying the displacement thickness could be achieved from this system.

Another reason why the new system is preferable to the one above is that in a numerical computation the numerical solution near the upper end of the range, i.e. for large $\tilde{y}$ can be seriously in error for the (28)–(30) system. This difficulty has been reported by Smith & Clutter (1962). The reason for this is that the first term in (29)

$$\frac{\partial\tilde{\psi}}{\partial\tilde{y}}\frac{\partial^2\tilde{\psi}}{\partial\tilde{x}\,\partial\tilde{y}}\sim q\frac{dq}{dx}+\text{exponentially small terms} \tag{31}$$

in the exact solution, and the first terms on the left- and right-hand sides of (29) cancel leaving exponentially small terms. However, in a numerical computation, since each quantity will be stored to an accuracy of, say, five significant figures, this accuracy will be completely lost when two quantities of almost equal magnitude are subtracted. For example, when the difference between the two terms should be of order 10^{-4}, accuracy of only one or two significant figures will be retained, while for larger values of $\tilde{y}$ the result can be orders of magnitude in error. The effect of this error on the other two terms in (29) can be appreciable and lead to great difficulties when trying to get convergence of the numerical solution for large values of $\tilde{y}$ (Smith & Clutter 1962).

One more advantage of the (23), (24) formulation is that the boundary-layer thickness remains of the same order of magnitude when using the variable η as we go downstream whereas when using the $(\tilde{x},\tilde{y})$ variables the boundary layer grows roughly as $x^{\frac{1}{2}}$, so that in the numerical computation extra points have continually to be fed in at the upper end of the range.

Another system which would seem to have the same advantages as the (23), (24) system can be obtained from (28) and (29) by writing

$$x^*=\tilde{x}, \quad y^*=(q/\tilde{x})^{\frac{1}{2}}\tilde{y}, \quad \tilde{\psi}=(\tilde{x}q)^{\frac{1}{2}}(\phi^*+y^*-\Delta^*), \tag{32}$$

where the dimensionless scaled displacement thickness $\tilde{\delta}_1=(\tilde{x}q)^{\frac{1}{2}}\Delta^*$. This leads to a third-order equation for ϕ^* and ϕ^* decays exponentially for large y^*. This system has been programmed and various computations have been performed, including runs past separation and reattachment. The separation program, however, was rather more involved than in the present system.

4. Stagnation point

We first consider the flow past a parabola whose equation in the z-plane is

$$y^2 = 2x + 1. \tag{33}$$

Here, the typical length L mentioned in § 2 by which all lengths are non-dimensionalized has been taken to be the nose radius of the parabola.

The transformation to the Z-plane is given by

$$z = \tfrac{1}{2}(Z+i)^2. \tag{34}$$

Hence

$$dz/dZ = Z + i,$$

and

$$J = \left|\frac{dz}{dZ}\right|^2 = X^2 + (Y+1)^2 = \frac{X^2+Y^2}{q^2} \tag{35}$$

from (16). Thus

$$J(X,0) = 1 + X^2, \quad q^2(X,0) = X^2 + \ldots. \tag{36}$$

Near the stagnation point of a symmetrical body the flow will be like that of a parabola near its stagnation point and we may write

$$J = 1 + \ldots. \tag{37}$$

The solution of (23) and (24) may now be found for small values of ξ. We assume that

$$H + \eta = F(\eta) + \ldots \tag{38}$$

and from (24), with $J = 1 + \ldots$, we have

$$-\bar{\omega} = F''(\eta) + \ldots, \tag{39}$$

where the primes denote differentiation with respect to η. Substituting these expressions in (23) we obtain a fourth-order differential equation for $F(\eta)$:

$$F^{\mathrm{iv}} + FF''' - F'F'' = 0,$$

which may be written in the more familiar form

$$[F''' + FF'' + 1 - F'^2]' = 0, \tag{40}$$

the well-known equation for the stagnation-point profile. The boundary conditions are, however, slightly different from the usual ones: they are in fact

$$F = F' = 0 \quad \text{for} \quad (\eta - \eta_B) = 0 \tag{41}$$

at the wall, and

$$F = \eta + \text{exponentially small terms} \tag{42}$$

for large η, since H must decay exponentially. The (non-dimensional) displacement thickness $\delta_1 = \lambda\Delta_s$ is given by

$$\Delta_s = \int_{\eta_B}^{\infty} (1 - F')\, d\eta = -\eta_B. \tag{43}$$

5. Numerical integration of the equations

Equation (23) can be treated as a parabolic equation for $\bar{\omega}$. If written in the form

$$\xi\left(1+\frac{\partial H}{\partial \eta}\right)\frac{\partial \bar{\omega}}{\partial \xi}=\frac{\partial^2 \bar{\omega}}{\partial \eta^2}+\left(\eta+\frac{\partial(\xi H)}{\partial \xi}\right)\frac{\partial \bar{\omega}}{\partial \eta}-\left(1+\frac{\partial H}{\partial \eta}\right)\bar{\omega}, \tag{44}$$

it may be seen that it resembles the simplest parabolic equation, the heat-conduction equation, except that the coefficient of $\partial\bar{\omega}/\partial\xi$ is non-constant, and there are also terms containing lower-order derivations added to the right-hand side.

For the numerical integration of (44) it is convenient to make a further transformation in order that the wall will pass through a mesh point, so avoiding the need to use an interpolation formula when applying the boundary conditions. We write

$$\bar{\eta}=(\eta+\Delta)/(\eta_0+\Delta), \quad \bar{H}=H/(\Delta+\eta_0), \tag{45}$$

where $\Delta=\Delta(\xi)=-\eta_B(\xi)$ and η_0 is a conveniently large constant chosen such that when $\eta=\eta_0$ both $\bar{\omega}$ and H are less than some small constant, say 10^{-5}. The integration in the η-direction will now conveniently range from $\bar{\eta}=0$ to $\bar{\eta}=1$.

Under this transformation (23) and (24) become

$$(\Delta+\eta_0)\left\{(\Delta+\eta_0)\left(1+\frac{\partial \bar{H}}{\partial \bar{\eta}}\right)\frac{\partial(\xi\bar{\omega})}{\partial \xi}-\left[(\bar{\eta}-1)(\Delta+\eta_0+\Delta'\xi)+\eta_0+\frac{\partial}{\partial \xi}(\xi(\Delta+\eta_0)\bar{H})\right]\frac{\partial \bar{\omega}}{\partial \bar{\eta}}\right\}=\frac{\partial^2 \bar{\omega}}{\partial \bar{\eta}^2}, \tag{46}$$

where Δ' denotes $d\Delta/d\xi$; and

$$-J\bar{\omega}=\frac{1}{\Delta+\eta_0}\frac{\partial^2 \bar{H}}{\partial \bar{\eta}^2}. \tag{47}$$

The boundary conditions (from (25)) are

$$\bar{H}=\frac{\Delta}{\Delta+\eta_0}, \quad \frac{\partial \bar{H}}{\partial \bar{\eta}}=-1 \quad \text{when} \quad \bar{\eta}=0, \tag{48}$$

and that $\bar{H}$ and $\bar{\omega}$ are exponentially small for large $\bar{\eta}$.

This latter condition is replaced by

$$\partial \bar{H}/\partial \bar{\eta}=\bar{H}=\bar{\omega}=0 \quad \text{when} \quad \bar{\eta}=1 \tag{49}$$

for the numerical solution.

Equation (47) may be integrated twice to give

$$\bar{H}=J(\Delta+\eta_0)\int_{\bar{\eta}}^{\infty}(\bar{\eta}-\eta_1)\bar{\omega}(\xi,\eta_1)\,d\eta_1, \tag{50}$$

or

$$\bar{H}=J(\Delta+\eta_0)\int_{\bar{\eta}}^{1}(\bar{\eta}-\eta_1)\bar{\omega}(\xi,\eta_1)\,d\eta_1 \tag{51}$$

for the numerical solution.

An implicit difference scheme similar to the Crank–Nicolson (1947) method was used and the difference problem solved by a matrix-factorization method as used by Leigh (1955). This difference scheme may be shown to be unconditionally

stable when applied to the heat-conduction equation and it is expected that it will be stable for all choices of step-lengths for the more complicated equation (46). In fact no instability was discovered up to the separation point. The truncation errors involved in this scheme are $O(\Delta\xi^2)+O(\Delta\bar{\eta}^2)$, where $\Delta\xi$ and $\Delta\bar{\eta}$ are the step-lengths in the ξ- and $\bar{\eta}$-directions respectively. Owing to the non-linear nature of (46) an iteration is necessary, the simplest way being to treat the coefficients of $\partial(\xi\bar{\omega})/\partial\xi$ and $\partial\bar{\omega}/\partial\bar{\eta}$ as known, solve the difference equation derived from (46) supplemented by the second of the conditions (48) applied to (51), and then obtain better approximations to these coefficients by calculating $\bar{H}$ from (51) and Δ from the first condition of (48) applied to (51). The whole process is repeated until the values obtained from two successive iterations agree to within some stipulated accuracy.

To begin the integration from the stagnation point, equation (40) with boundary conditions (41) and (42) must be integrated and it was found necessary to use a series solution, similar to Görtler's (1957) series, in order to find the solution at some small distance from the stagnation point before using the marching technique described above.

6. Examples

6.1. *Parabola*

This example is included to demonstrate and check the method.

A parabolic displacement surface was considered with unit radius of curvature at the nose. The transformation formulae were given in § 4 and we take

$$J = \xi^2+(1+\lambda\eta)^2, \tag{52}$$

from (35) and (21). If infinite Reynolds number is taken, (52) becomes

$$J = 1+\xi^2. \tag{53}$$

With this expression for J the equations were integrated as in § 5 from $\xi = 0{\cdot}2$ to $\xi = 5$, using the series expansion to obtain the profile at $\xi = 0{\cdot}2$.

Figure 3 shows values of Δ, q and $-\lambda\omega_0$ as functions of $\xi (0 \leqslant \xi \leqslant 5)$. $\Delta (= -\eta_B(\xi))$ is related to the (non-dimensional) displacement thickness δ_1 by the expression

$$\Delta = \delta_1/(\lambda J^{\frac{1}{2}}). \tag{54}$$

$-\lambda\omega_0 (= -\xi\bar{\omega}(\xi, \eta_B))$ the 'scaled' value of the vorticity on the body, is related to the skin friction τ_w by

$$-\lambda\omega_0 = \frac{1}{\lambda}\frac{\tau_w}{\rho U_\infty^2}, \tag{55}$$

and the magnitude of the velocity of the potential flow along S_D is

$$q = \xi/J^{\frac{1}{2}} \tag{56}$$

from (16) and (21) with $\eta = 0$.

Far downstream we may write, for large ξ,

$$J \sim \xi^2, \tag{57}$$

and look for a solution of the form

$$H+\eta = F(\eta), \quad -\bar{\omega} = F''/\xi^2 \tag{58}$$

from (24), where the primes denote differentiation with respect to η.

Substituting these expressions into (23) and integrating once we arrive at the well-known Blasius equation

$$F''' + FF'' = 0, \tag{59}$$

with boundary conditions

$$F = F' = 0 \quad \text{for} \quad \eta = \eta_B = \eta_B(\infty) \tag{60}$$

and

$$F = \eta + \text{exponentially small terms} \tag{61}$$

for large η. When (59) is solved with these boundary conditions we find

$$-\eta_B(\infty) = \Delta(\infty) \doteq 1{\cdot}2167.$$

The asymptotic values of q and ω_0 are, from (56), (57) and (58), unity and zero respectively.

With $\lambda = 0$ the body and displacement surface are coincident in the physical (x, y)-plane, but if we assign a finite, but small, value to λ the results from the

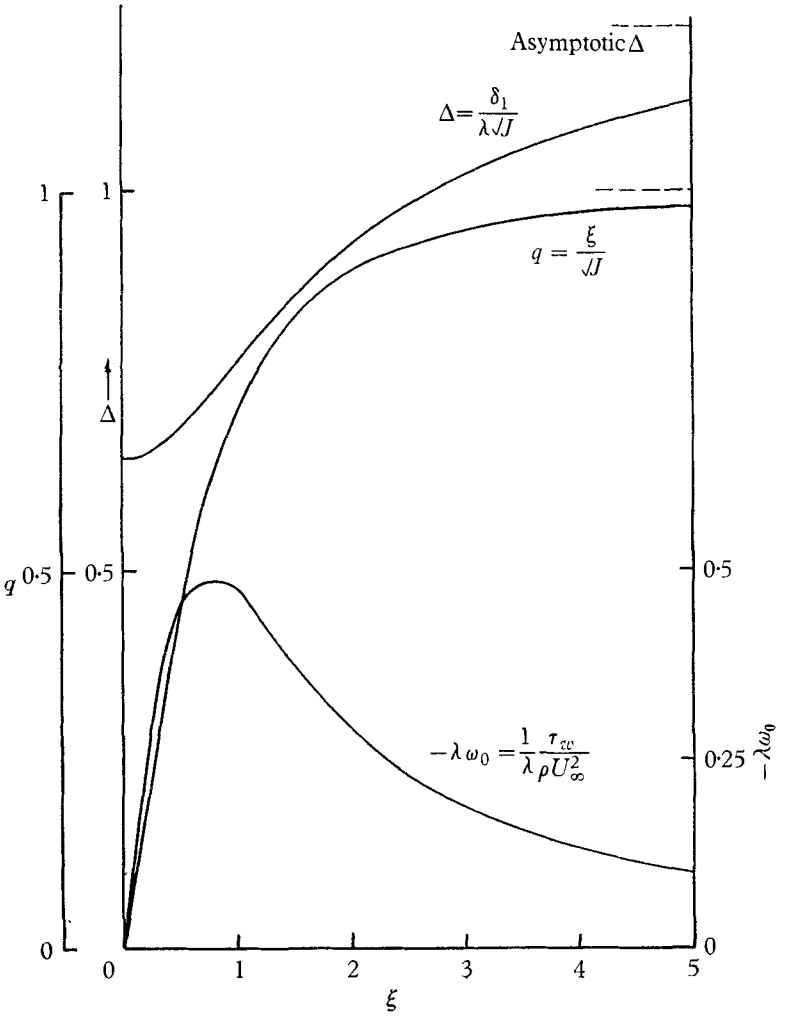

FIGURE 3. The flow parameters Δ, q and $-\lambda\omega_0$ for the case of a parabolic displacement surface.

(ξ, η)-plane can be interpreted in the physical plane to give a picture for a flow at large but finite Reynolds number. With a non-zero value for λ equations (23) and (24) do not give an exact solution of the Navier–Stokes equations but can be considered to give a first approximation for small λ.

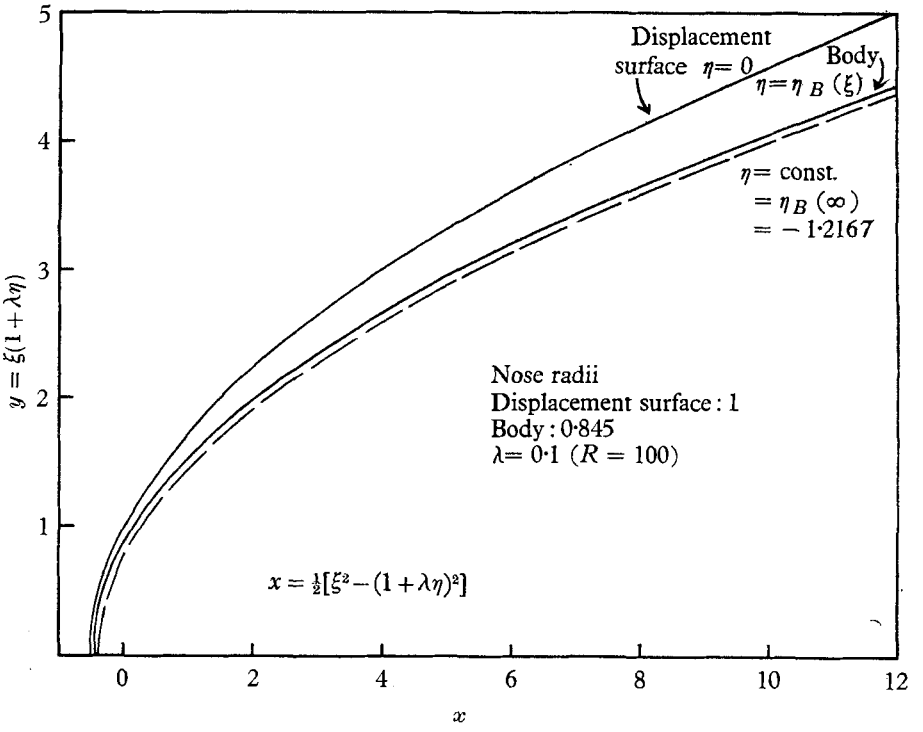

FIGURE 4. Body giving rise to a parabolic displacement surface for $\lambda = 0{\cdot}1$.

Figure 4 shows the results obtained for a parabolic displacement surface for $R = 100$. The broken line is another parabola with the same focus as the displacement surface, and with which the body is asymptotically coincident far downstream. This figure is meant as an illustration rather than as an exact mathematical result.

6.2. *A flow containing an adverse pressure gradient*

The following distribution was assumed for q:

$$q = q_0 + q_1(\xi - \xi_0) - q_2(\xi - \xi_0)^2, \tag{62}$$

where $q_r > 0$. For simplicity the initial profile was obtained assuming a parabolic displacement surface up to $\xi = \xi_0 = 0{\cdot}2$ and then the values of q_0 and q_1 chosen so that at $\xi = \xi_0$ both q and $dq/d\xi$ were continuous, q_2 may be chosen so as to give a velocity maximum at any required value of ξ.

We note here that if ξ is replaced by $\alpha\bar{\xi}$ and q by $\alpha\bar{q}$, where α is a constant, equations (23) and (24) and the value of J from (27) remain unchanged. This means that after a computation has been performed using a specified set of values

for J the results may be interpreted in a number of ways. For instance ξ and q could be scaled to give a maximum value for q of any value we please. However, if any scaling is performed the results will no longer correspond to a displacement surface having unit radius of curvature at the nose.

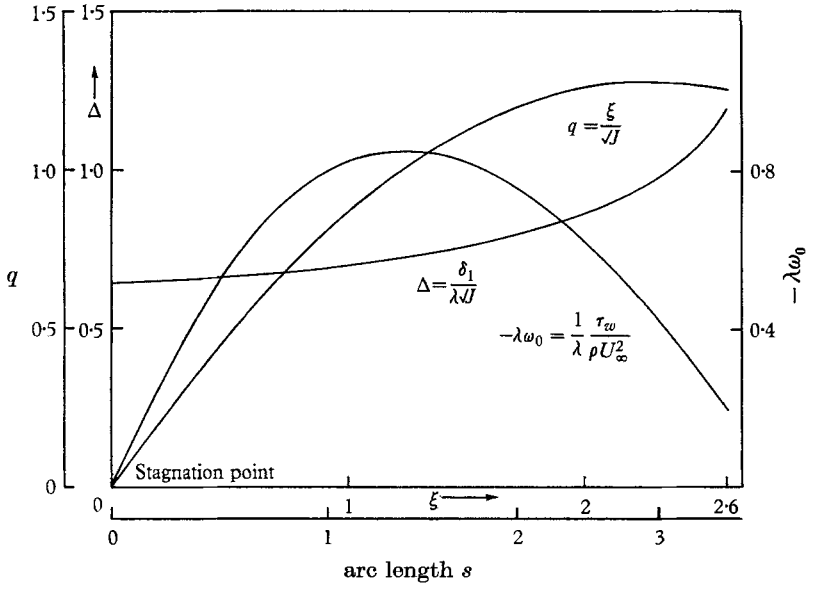

FIGURE 5. Computation from stagnation point—(q prescribed).

Values of Δ and $-\lambda\omega_0$ for the specified q distribution (62) up to $\xi = 2{\cdot}6$ are shown in figure 5. To relate these curves to the physical plane a grid showing the arc length along S_D is included in figure 5. The arc length s is calculated from

$$ds^2 = J(dX^2 + dY^2), \tag{63}$$

which, for $\lambda = 0$ (from (16) and (21)) becomes

$$ds = (\xi/q)\,d\xi. \tag{64}$$

Soon after $\xi = 2{\cdot}6$ the iteration procedure used in the computation began to fail. The convergence criterion that was used for the iteration scheme was that if the values of Δ obtained from two successive iterations are Δ^p and Δ^{p+1} then the solution is considered to have converged when

$$|\Delta^p - \Delta^{p+1}| < C, \tag{65}$$

where C is some small constant less than the truncation error. There would seem to be a choice as to which of the boundary conditions (48) is to be applied to (51) to supplement the difference equation obtained from (46) in order to find ω (the other boundary condition of (48) is used with (51) to determine Δ from the values of ω obtained). Near the stagnation point it was found that if the first of (48) was used to find ω then the iterations diverged, whereas if the second was used, successive values of Δ^p approached the true value rapidly in a monotonic fashion. However, after $\xi = 2{\cdot}6$ successive values of Δ^p approached the true value more

and more slowly. This means that it is very difficult to ascertain the true value of Δ, since if Δ^p and Δ^{p+1} both lie on the same side of the true value, then (65) could be satisfied while Δ^p and Δ^{p+1} are both far from the true value. Strictly speaking (65) will be an insufficient condition for convergence everywhere if the true value is approached monotonically. However, in areas where the convergence was fast, various values of C were fed in and results compared. With a value of C of 10^{-4}, successive values agreed to within 10^{-4} after about six iterations. With $C = 10^{-5}$ and 10^{-6}, respectively, two and four more iterations were needed, but the final values were less than 10^{-5} greater than their values after the sixth iteration. The true value could only be obtained by making C tend to zero, but it seems very unlikely that this would improve much on the value found with $C = 10^{-4}$. Hence these values were accepted in the area of rapid convergence. The value of $|\Delta^{p+1} - \Delta^p|$ for a fixed p became smaller as the separation point (where $\omega_0 = 0$) was approached and so the problem of convergence of the iteration scheme becomes more acute as we approach the separation point.

Using the first of the conditions (48) to find ω away from the stagnation point it was found that the values of Δ from successive iterations oscillated about the true value, a much more satisfactory state of affairs, since when (65) is satisfied we know that both Δ^p and Δ^{p+1} are within C of the true value. However, near separation successive values of Δ failed to converge. The other method (using the second of the conditions (48) to find ω) also failed to converge near separation. Prior to this Δ had begun to increase more rapidly and it is thought that the presence in equation (46) of the term $\Delta'\xi$ probably accounts for the instability of the iteration scheme, since if, during the iteration, Δ' becomes very large this term will dominate and change the nature of the equation. Consequently a new scheme was sought.

6.3. *Integration past the separation point*

A glance at equations (46) and (47) shows that both J and Δ occur in the equations. Up to now J ($= \xi^2/q^2$) has been specified and Δ has remained to be calculated along with H and ω. However, the present method allows for the roles of J and Δ to be reversed so that Δ can be specified, leaving J to be determined from the integration.

On reflexion, this seems a reasonable technique since it now allows the potential flow to be modified, through q, whereas usually q is calculated on the assumption that there is no separation, or at least that there is no sudden thickening of the boundary layer, and is expected to be unaffected by separation. This could possibly account for the singularity usually encountered at the separation point, the suggestion being that the singularity is not inherent in the boundary-layer equations but is introduced when the outer boundary condition in the form of a specified q is expected to behave as though there were no separation.

The first case tried was to write

$$\Delta = d_0 + d_1(\xi - \xi_1) + d_2(\xi - \xi_1)^2, \tag{66}$$

where $d_k > 0$ and ξ_1 is some starting point, taken as 2·6. d_0 and d_1 were chosen to make Δ and $d\Delta/d\xi$ continuous at $\xi = 2{\cdot}6$. Three values of d_2 were tried, repre-

sented by the curves A, B and C in figure 6. The corresponding values of q and $-\lambda\omega_0$ obtained from the integration are also plotted on figure 6. In each case no difficulty was encountered in passing through separation.

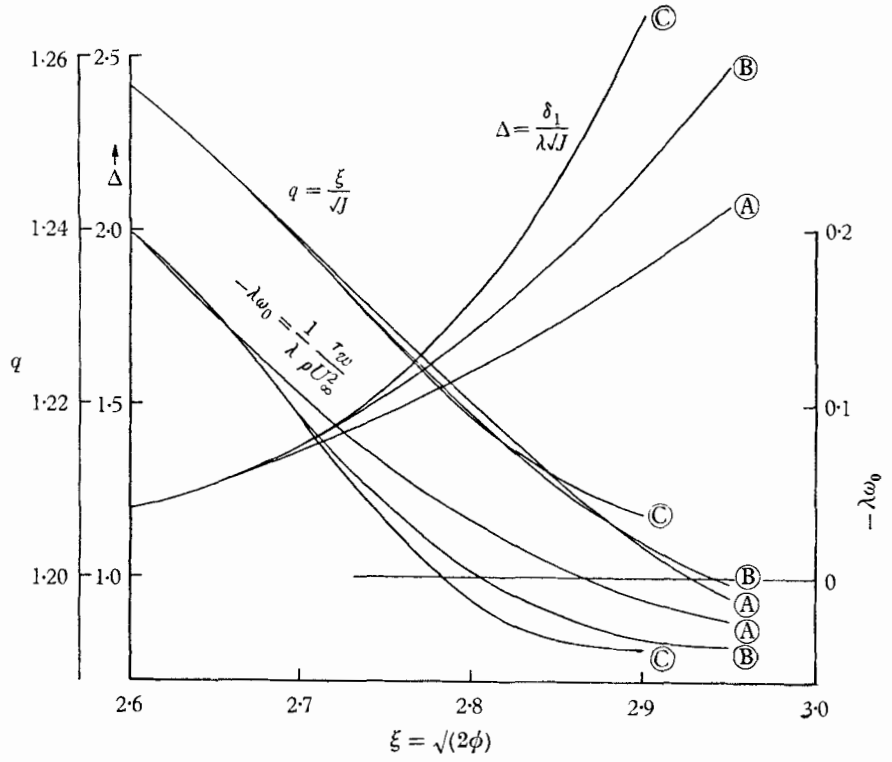

FIGURE 6. Δ, q and $-\lambda\omega_0$ curves for three cases round separation (Δ prescribed).

It may be noted here that although the values of q obtained differ in these three cases this does not necessarily mean that the bodies (or rather the displacement surfaces) giving rise to these flows differ in this region. A knowledge of q along the whole length of S_D is necessary before the body shape corresponding to it can be calculated. If we take the logarithm of the inviscid complex velocity $q\,e^{-i\tau}$ along S_D, the real and imaginary parts of this analytic function are linked, and by Cauchy's theorem $\tau(\xi, 0)$, which gives the body shape, is given by

$$\tau(\xi, 0) = \frac{1}{\pi}\int_{-\infty}^{\infty} \frac{\log q(\xi', 0)}{\xi' - \xi}\, d\xi', \tag{67}$$

so that although at a particular value of ξ the values of q obtained from A, B and C may differ, the values of τ at that point can be identical provided the values of q differ in some suitable fashion in some other region. In other words, three bodies could be identical up to any given station, but have differing q distributions up to there because the bodies differ downstream of this station.

The streamline pattern for the case C is shown in figure 7. Because of the co-ordinate system chosen, the displacement surface appears in this figure as the line $\eta = 0$, and the body as a curve. For comparison some streamlines of the

inviscid flow are included (the broken lines). At $\eta = 2$ the viscous and inviscid flows differ only in the third significant figure (i.e. $H = O(10^{-2})$). The integration was actually performed up to $\eta = 4$, where the viscous term H was down to about 10^{-8}.

Also included in figure 7 are the lines $\partial\psi/\partial\eta = 0$ and $\omega = 0$, representing the locus of points at which the component of the velocity normal (in the (ξ, η)-plane) to the isobars is respectively zero and has its maximum negative value.

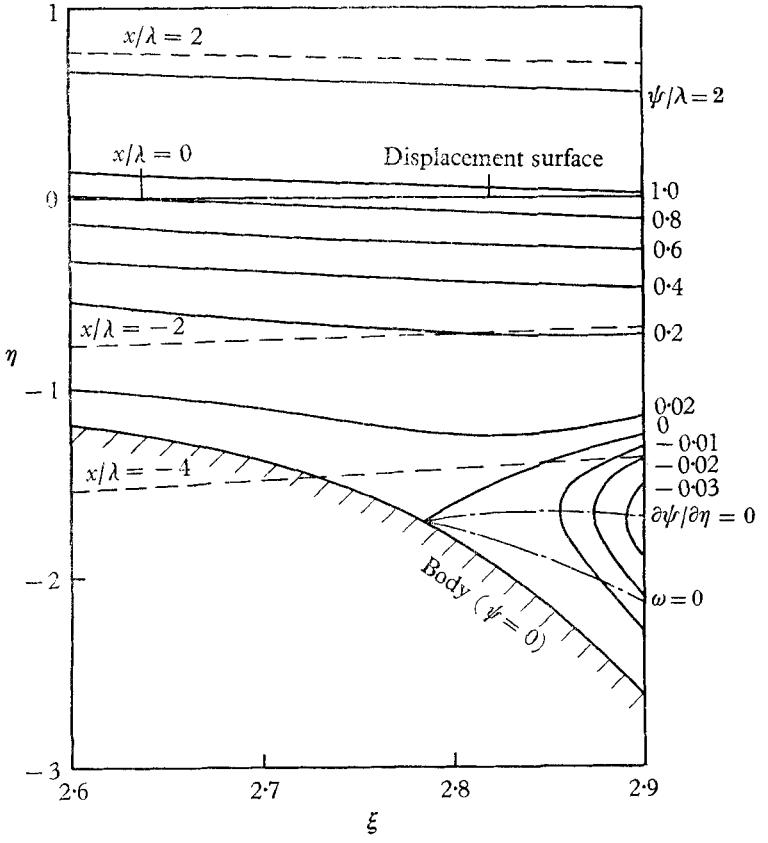

FIGURE 7. Flow pattern near separation point (Δ prescribed).
—, Streamlines of the viscous flow; – – –, streamlines of the inviscid flow.

Velocity profiles just upstream and just downstream of separation are shown in figure 8. It may be seen that the velocity within the reversed-flow region is relatively small.

After about $\xi = 2{\cdot}9$ difficulty was again encountered with the iteration. The tolerance (C in (65)) was put at 10^{-4} and it was found that at $\xi = 2{\cdot}95$ successive values of J in the iteration would not converge to within this tolerance, although they would converge to within a larger tolerance (10^{-2}). This is possibly to be expected, since the region of reversed flow should really be integrated in the negative ξ-direction with boundary conditions provided from downstream. This means that there is no unique solution if the integration is performed in the

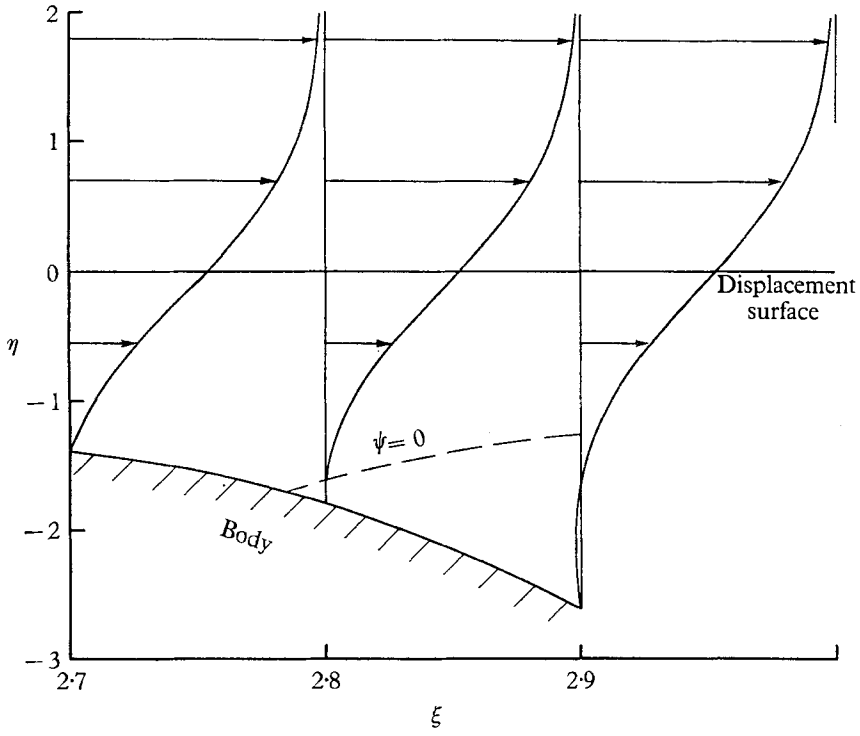

FIGURE 8. Velocity profiles near separation point.

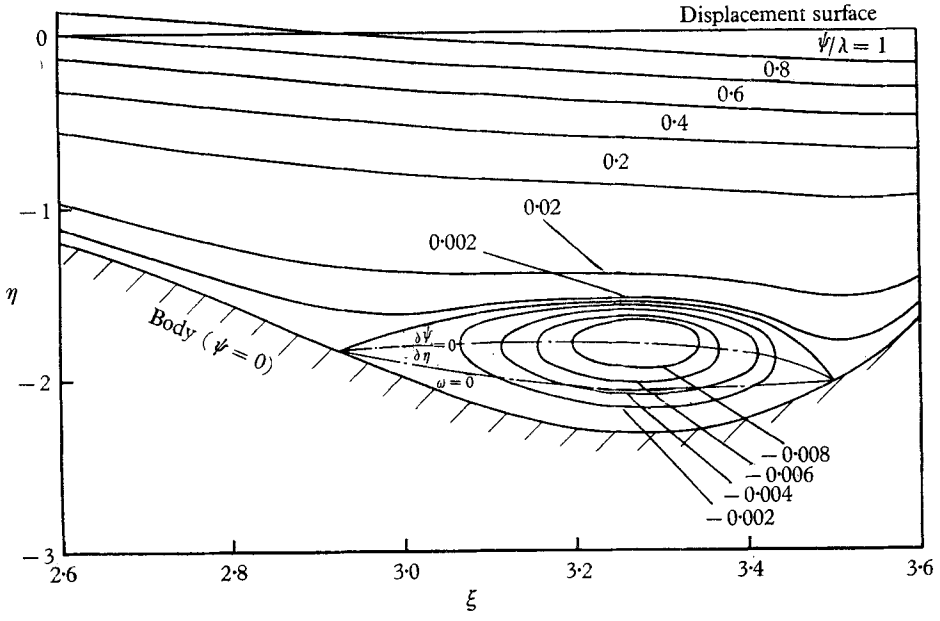

FIGURE 9. Flow pattern round attached bubble—(Δ prescribed).

positive ξ-direction, although we can say that all the possible solutions at $\xi = 2{\cdot}95$ appear to lie within 10^{-2} of each other, and at $\xi = 2{\cdot}9$ within 10^{-4} of each other. An alternative might be to 'guide' the solution by considering it as a perturbation of a known self-similar solution far downstream. Of course, if there is no steady-flow solution after separation this instability in the iteration scheme may point to the onset of instability in the flow downstream of separation.

6.4. *Integration past separation and reattachment*

Next a convex/concave Δ-distribution was fed in of the form

$$\Delta = a_0 + a_1(\xi - \xi_1) + a_2(\xi - \xi_1)^2 - a_3(\xi - \xi_1)^3, \tag{68}$$

where $a_k > 0$ and ξ_1 is some starting point, taken as 2·6. a_0 and a_1 were chosen to make Δ and $d\Delta/d\xi$ continuous at $\xi = 2{\cdot}6$.

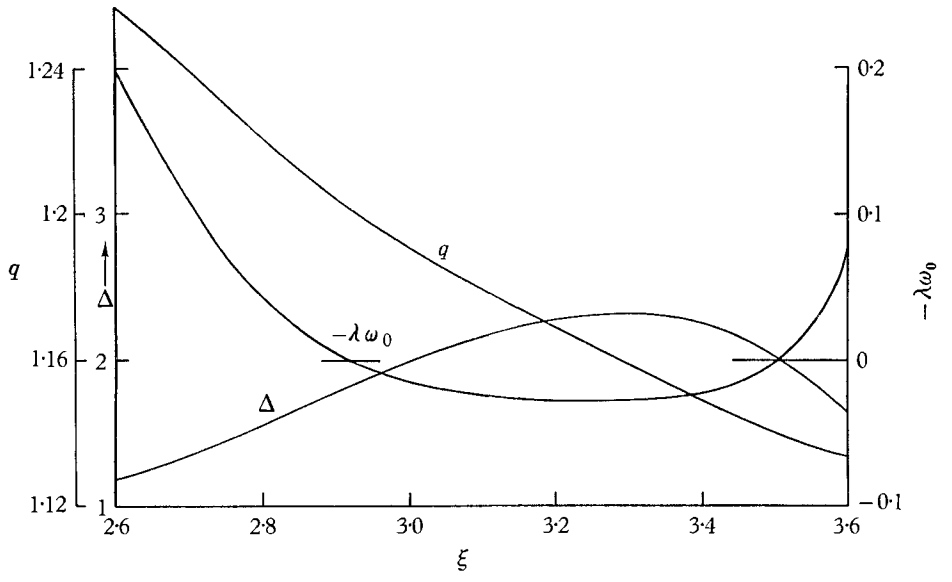

FIGURE 10. Δ, q and $-\lambda\omega_0$ curves for attached bubble.

With this distribution separation and reattachment were obtained, the streamline pattern being shown in figure 9 and q and $-\lambda\omega_0$ curves in figure 10. In this case the iterations at each step converged to within the desired tolerance, 10^{-4}, so that, although, as mentioned above, the solution found cannot be considered to be the unique solution, all the possible solutions appear to lie within 10^{-4} of each other.

As a check the integration was repeated using three different step-lengths b in the ξ-direction: $b = 0{\cdot}05$, $0{\cdot}025$ and $0{\cdot}0125$. For the latter two step-lengths the values of q obtained agreed to within 10^{-4}, and the values for $b = 0{\cdot}05$ and $b = 0{\cdot}025$ (or $0{\cdot}0125$) to within 10^{-3}. Similar agreement was found between the values of $-\lambda\omega_0$ obtained.

6.5. *Discussion of flow near a separation point*

In the (X, Y)-plane (see § 3) we assume that the flow near the separation point can be represented by regular expansions in powers of X and Y. The wall may be represented by the line $Y + aX = 0$, and the separating streamline by the line

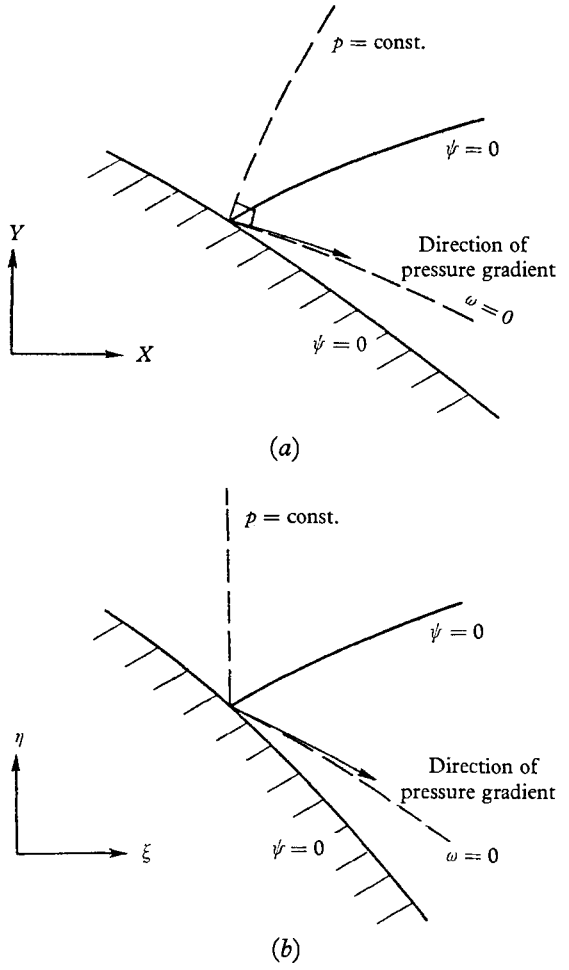

FIGURE 11. Schematic picture of the isobar, separating streamline, pressure-gradient direction and zero vorticity lines at the separation point. (*a*) (X, Y)-plane; (*b*) (ξ, η)-plane.

$Y + bX = 0$, where the separation point is taken as the origin ($X = 0$, $Y = 0$) (figure 11 (*a*)). Thus, since ψ has a double zero at the surface

$$\psi = c(Y + aX)^2(Y + bX) + \ldots \tag{69}$$

near the separation point. a, b and c are constants. When the co-ordinate Y is 'stretched' the equivalent relation to (69) in the (ξ, η)-plane can be obtained by scaling the various quantities in (69) thus:

$$\psi = \lambda\bar{\psi}, \quad Y = \lambda\eta, \quad X = \xi, \quad a = \lambda\bar{a}, \quad b = \lambda\bar{b}, \quad c = \bar{c}/\lambda^2, \tag{70}$$

resulting in the relationship

$$\overline{\psi} = \bar{c}(\eta + \bar{a}\xi)^2(\eta + \bar{b}\xi) + \ldots \tag{71}$$

(figure 11(*b*)).

From (20), (70) and (71) the leading terms for small λ for the vorticity near separation are given by

$$-J\lambda\omega = 2\bar{c}[3\eta + (\bar{b} + 2\bar{a})\xi] + \ldots.$$

Hence the slope of the curve $\omega = 0$ at the separation point is

$$d\eta/d\xi = -\tfrac{1}{3}(\bar{b} + 2\bar{a}). \tag{72}$$

The slopes of the surface and separating streamline at the separation point are

$$d\eta/d\xi = -\bar{a}, \tag{73}$$

and

$$d\eta/d\xi = -\bar{b}, \tag{74}$$

respectively.

A computation using small step-lengths was performed in the neighbourhood of the separation point for the case considered in (6.4) above. From the slopes of the surface and separating streamline values of $\bar{a}$ and $\bar{b}$ were obtained from (73) and (74). Within the accuracy of the computation the value of the slope of the line $\omega = 0$ from (72) agreed with the value found from the computation. This shows that a regular expansion at separation fits the numerical results and therefore gives some justification for the assumption of a regular behaviour of the flow near separation.

Legendre (1955) shows (using the full Navier–Stokes equations) that at the surface of a body the direction of the pressure gradient is parallel to the direction of the lines of constant vorticity (constant ω) and in addition, at a regular separation point, the tangent of the angle between this direction and the surface is one-third of the tangent of the angle between the separating streamline and the surface. These results can be derived from (69). They do not contradict the relations given above for the plane of the stretched variables, since angles are distorted by the stretching.

REFERENCES

Catherall, D., Stewartson, K. & Williams, P. G. 1965 *Proc. Roy. Soc.* A, **284**, 370.
Crank, J. & Nicolson, P. 1947 *Proc. Camb. Phil. Soc.* **43**, 50.
Goldstein, S. 1948 *Quart. J. Mech. Appl. Math.* **1**, 43.
Görtler, H. 1957 *J. Math. Mech.* **6**, 1.
Leigh, D. C. F. 1955 *Proc. Camb. Phil. Soc.* **51**, 320.
Legendre, R. 1955 *Comptes Rendus* **241**, 732.
Smith, A. M. O. & Clutter, D. W. 1962 *Douglas Aircraft Co. Inc. Engng Paper*, no. 1530.
Stewartson, K. 1958 *Quart. J. Mech. Appl. Math.* **11**, 399.
Terrill, R. M. 1960 *Phil. Trans. Roy. Soc.* A, **253**, 55.
Van Dyke, M. D. 1962 *J. Fluid Mech.* **14**, 161, 481.
Van Dyke, M. D. 1964 *J. Fluid Mech.* **19**, 145.